DTU Fotonik
Department of Photonics Engineering

DTU

Fiber Optical Parametric Oscillator

Enric García Sánchez (s142295)
Master Thesis
Kongens Lyngby
24th February 2015

Supervisors:
Jesper Lægsgaard
Sidsel Rübner Petersen
Thomas Tanggaard Alkeskjold
Christina B. Olausson
Johannes Weirich

NKT Photonics
the power of light

Abstract

The parametric gain of a four-wave mixing (FWM) process in a configuration of a fiber optical parametric oscillator (FOPO) is one option to achieve the conversion of high peak power pulses at frequencies reachable with rare-earth doped fibers. The point is that rare-earth doped fiber lasers and amplifiers have restrictions in the wavelength coverage due to the available dopants and their electronic transitions. Thus, to extend this coverage, silica fibers are being used as nonlinear media to aid the frequency conversion process.

The FOPO considered in this project consists of a 40 ps 1064 nm high peak-power pump laser, a well-characterized hybrid photonic crystal fiber (PCF) and a feedback system. Via FWM the pump frequency is converted into new frequencies in the PCF, which can be feed back into the PCF and amplified, thereby creating a FOPO.

The pump is converted to 1140 nm and 1000 nm through FWM in the hybrid PCF, and, even though all the components go through the FOPO recirculation system, only the 1000 nm component goes back into the hybrid PCF. The whole setup is based on free-space optics.

Preface

This is a 30 ECTS points master thesis project started on September 1st, 2014 and finished on January 21st, 2015. The experimental part of this project has been performed in the laboratories of NKT Photonics and at the DTU Fotonik department. It has been supervised by PhD student Sidsel Rübner Petersen and Associate Professor Jesper Lægsgaard from DTU, and PhD Thomas Tanggaard Alkeskjold and R&D engineer Christina B. Olausson from NKT Photonics.

There is many people I would like to give thanks at this point. First of all, my parents, because they gave me the opportunity to study abroad and it has been a great experience.

Sidsel Rübner Petersen for her time supervising my work in the laboratory and all her pieces of advice, and Johannes Weirich for volunteering to take Sidsel's place, during my last days at NKT Photonics. Associate Professor Jesper Lægsgaard, PhD Thomas Tanggaard Alkeskjold and R&D engineer Christina B. Olausson for their guidance during the project and their willing to solve the problems we had along the way.

All my friends, the ones from Spain who kept in contact on my time in Denmark to cheer me up and came to visit me: Cristian Bernad, María Machimbarrena, Clara Torrecillas, Olga Masvidal, Ismael Serrano, Ismael Hernández, Alexandra Caparrós, Helena Pizarro, Disney González and Cristina Ródenas, and the ones I am really glad I met there and made my stay more comfortable and easier, my Spanish crew: Alberto Prieto, Daniel Cascales and Sandra López, and my international buddies: Anthony Economou, Kristian Freng Svendsen, Ilsur Khusainov, Ippei Takeuchi, Robert May, Tibbe Titulaer, Karol Dzitkowski and Marco Agosti.

Finally, special thanks to my girlfriend Tamar Galán, for her patience along this adventure and her ability to get the problems out of my mind.

Contents

Abstract **i**

Preface **iii**

1 Introduction **1**
1.1 Motivation 2
1.2 Goals 3

2 Photonic Crystal Fibers **5**
2.1 Index-guiding Fibers 5
2.2 Bandgap Guidance Fibers 6
2.3 Hybrid Photonic Crystal Fibers 7

3 Four Wave Mixing **11**
3.1 Main Theory 11
3.2 Phase-Matching 14
3.3 Parametric Amplification 15

4 Laboratory Work **21**
4.1 The setup 21
4.2 Laser and FOPA characterization 24
4.3 Establishing the recirculation 29

5 Conclusion and Outlook **35**
5.1 Outlook 36

Appendix **37**

A Matlab Codes for Parametric Gain Calculations **37**

Bibliography **43**

Chapter 1

Introduction

The use of photonic bandgap fibers (PBGFs) allows distributed spectral filtering (DSF) to eliminate long- and short-wavelengths amplified spontaneous emission (ASE). In the case of hybrid photonic crystal fibers (PCF), a total-internal reflection guiding fiber can be created with the spectral properties of PBGFs due to the airholes and high-index rods combination, where the first ones provide index-guiding granting the design of large mode area (LMA) cores, without jeopardizing the single mode behaviour, while the high-index rods supply bandgap guiding resulting in gain shaping. In amplifier systems, the cancellation of ASE, stimulated Raman scattering (SRS) and/or FWM can be achieved with LMA fibers with DSF that provide flexibility in width and center wavelength design of the transmission band, given the use of spatially confined resonant structures, leading to spectral filtering, high-order modes suppression and polarization maintaining and compact coiling properties. The transmission bands in LMA hybrid PCFs can be adjusted giving great control of the transmission properties in spontaneous degenerate FWM. At the edges of a transmission band, the group velocity dispersion experiences considerable rise: in the blue edge results in large normal dispersion while in the red edge gives large anomalous dispersion. Therefore, in LMA hybrid PCF dispersion profile can be controlled adjusting the transmission bands, what yields spectral control of FWM components. FWM products can be generated within the transmission band with high peak power through a proper design of the LMA fiber maintaining single mode properties. To sum up, wavelength coverage of high power fiber sources can be enlarged by means of FWM in LMA hybrid PCFs [1, 2, 3].

Some progress on the field has been made in other ways. Access to femtosecond-scale pulses, by means of anti-Stokes chirped pulses re-compression, has been achieved in a parametric wavelength converter for the near-visible light where a polarization maintaining (PM) PCF was pumped with an external cavity laser diode (ECLD) fiber amplified seed, tunable in wavelength, repetition rate and pulse duration. This development can be useful for bio-

photonic applications. Besides, high conversion efficiency, broad bandwidth and dispersive waves (DWs) centered in two coherent anti-Stokes Raman scattering (CARS) regions provide high resolution for detection in biology and chemistry fields. This is attained through soliton self-frequency shift (SSFS) in a PM PCF with two zero-dispersion wavelengths, generating broadband blue- and red-shifted DWs. Moreover, using PM PCFs with different dispersion parameters and pumping near the ZDW of the fiber, and considering the polarization contribution, solutions based on the phase mismatch expansion in Taylor series for frequency shifts of the pump-divided vector FWM have been found, what leads to optimization of the parametric generation process because they allow a better understanding of the variation of fiber parameters' influence on the phase-matching curves [4, 5, 6].

1.1 Motivation

In recent years, rare-earth-doped fiber lasers and amplifiers have attracted a lot of attention, and a large power scalling has been carried out, especially in Yb-doped fibers. However the spectral range of rare earth doped silica fibers is naturally restricted by the available dopants.

The figure 1.1 shows the wavelength coverage of rare-earth-doped silica fibers in the near infrared. It is plain to see that there are some regions where the available rare-earth dopants are simply not sufficient to cover the full spectral range. And these regions have some interesting applications, for example within spectroscopy.

The point in working with a FOPO setup is that the frequency conversion given by the FWM is more efficient than in a FOPA. The difference between a FOPA and a FOPO relies on the FWM components generation. In a FOPA, spontaneous FWM is origined and the FWM components are built up from noise. In a FOPO stimulated FWM occurs, which can result in much higher

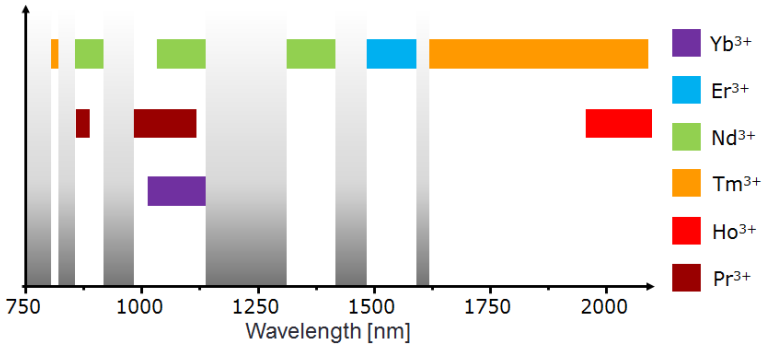

Figure 1.1: Wavelength coverage of rare-earth-doped silica fibers in the near infrared

generation efficiencies. Rare-earth doped amplifiers are restricted by the fluorescence of the rare-earth dopants. However, parametric amplifiers can cover all wavelengths, since they are not restricted by electronic transitions and fluorescence of the existing molecules.

1.2 Goals

In this project, a FOPO configuration is considered. The setup has two stages: the FOPA and the recirculation circuit. Three main goals rule the project. First of all, to achieve FWM around 1000 nm and 1140 nm in the FOPA, where the 1140 nm is the desired component. After optimizing the FOPA setup, the point is to recirculate the 1000 nm wave and reenter it to the FUT to give more power to the 1140 nm component. Finally, to fix the correct the recirculating wave delay in order to go into the FUT at the same time the pump pulse reaches the input of the fiber, so that the conversion efficiency is maximum.

Chapter 2

Photonic Crystal Fibers

Unlike conventional fibers with radially symmetric index distributions, the photonic crystal fibers are optical fibers that have a sophisticated structure on the μm scale with a transverse refractive-index profile. The microstructure can consist of an array of airholes along the length of the fiber, a pattern of doped and undoped sections or even a combination of both methods. The term 'crystal fibers' is due to the well-organized structure in the cladding region that most of them present [7].

Their properties can be tailored by the designer given the refractive-index difference between glass and air and the structural flexibility they offer, which is the main advantage in front of common optical fibers [7].

2.1 Index-guiding Fibers

A triangular pattern of airholes shape the cladding of this fibers and the absence of one or a small number of airholes determine the high-index core, providing the reflection at the interface between the cladding and the core. The distance between holes' center and the hole diameter are the parameters that define these fibers. An image of the cross section is shown in figure 2.1, on the left. They are called 'index-guiding' fibers because of their similarities to step-index fibers. They both share properties like supporting fundamental mode guidance at all frequencies [7].

Nonetheless, they have important differences. The propagating modes of a microstructured cladding material have the form:

$$\mathbf{H}(\mathbf{r}, t) = \mathbf{h}(x, y)exp(j(\omega t - \beta z)) \tag{2.1}$$

similar to the plane wave forms in a homegeneous material, but with the microstructure $\mathbf{h}(x, y)$ periodicity. According to the homogeneous material model, the highest effective index of the cladding mode is used as the cladding

index value. Similarly to the step-index relation for single-mode condition,

$$V \equiv \frac{2\pi\Lambda}{\sqrt{3}\lambda}\sqrt{n_c^2 - n_{cl}^2} \lesssim 2.4 \tag{2.2}$$

where $\Lambda/\sqrt{3}$ is replacing the core radius, a [7].

For long wavelengths, the effective index tends to the average value of silica and airholes, because, in the transverse plane, light has an uniform field distribution. The effective index grows while the wavelength diminishes, given the fact that the light starts to avoid the airholes. Finally, for short wavelengths, the effective index tends to the silica index, so the field is well confined to the silica part of the cladding. Using the scalar wave equation and the fundamental cladding mode as its solution, the following formula can be obtained:

$$n_{SiO_2}^2 - n_{eff}^2 = (\frac{\lambda}{2\pi})^2 \frac{\int \delta\mathbf{r}_\perp |\bigtriangledown_\perp \Psi|^2}{\int \delta\mathbf{r}_\perp |\Psi|^2} \tag{2.3}$$

what means that $n_{SiO_2}^2 - n_{eff}^2 \propto \lambda_2$, so

$$V_{PCF} = \frac{2\pi\Lambda}{\sqrt{3}\lambda}\sqrt{n_{SiO_2}^2 - n_{eff}^2} \sim constant \tag{2.4}$$

is the short-wavelength limit. This value depends on the d/Λ ratio, which assures single-mode behaviour at all wavelengths in case of being lower than 2.4. This case is attained for a d/Λ ratio of ~ 0.42, although for values lower than 0.5 these fibers are considered single-moded at all wavelengths [7].

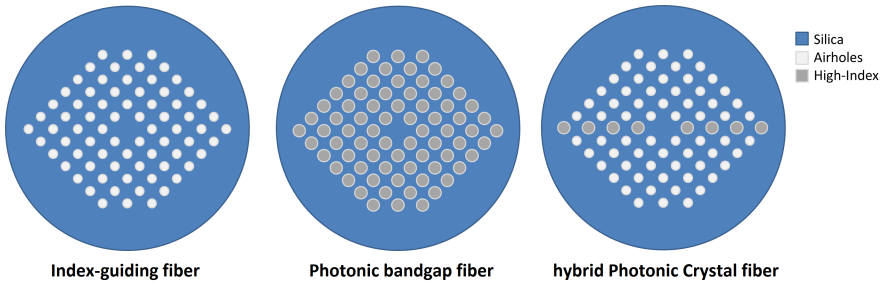

Figure 2.1: An example of each of the fibers discussed in this chapter. The left cross-section belongs to an index-guiding fiber. A photonic bandgap fiber cross-section can be seen in the center. Finally, the cross-section of a hybrid photonic crystal fiber is shown on the right.

2.2 Bandgap Guidance Fibers

The photonic band gaps (PBG) are the forbidden frequency windows, in all directions, by an array of airholes due to the interference effects, given the

large index contrast between the airholes and the material. The radiation can be captured at certain defects in the grid of scattering centers in PBG structures [7].

This effect cannot occur for in-plane propagation in both polarization directions at the same time, since the silica and air index difference is not large enough. But it can happen when considering out-of-plane propagation in a PCF. If the propagation constant of the fiber is large enough, small index steps can become efficient scattering centers in the transverse plane. Hence, particular values of propagation constants are forbidden for an specific frequency. Modes localized at these prohibited propagation constants can be trapped using imperfections in these PBG structures. The cladding of a PBG fiber consist of an array of high-index inclusions. It can be seen an image of the cross section of these kind of fiber in figure 2.1, in the center [7].

The main difference between PBG fibers and index-guiding PCF is that the core index must be lower than the cladding index, in the first ones, because they have larger effective index in cladding modes than in the guided mode, which means that they can be used for light guidance in low-index materials. Furthermore, they only guide in specific frequency bands, a few of which only allow higher-order modes but not the fundamental one [7].

2.3 Hybrid Photonic Crystal Fibers

Hybrid PCFs take advantage of the pros of both guiding methods. These fibers combine in one fiber the two guiding mechanisms at the same time: index-guiding and bandgap guidance. The core mode agrees with an index-guiding PCF one for wavelengths inside the bandgap, while it is filtered out otherwise, coupling to the cladding bands of the high-index inclusions. The confinement loss has an average value of the two guiding methods [8].

They have birefringence due to the different refractive indices of the materials in the two axes. Two orthogonally polarized modes can be hold even being SM fibers. The two axes with biggest refractive indices difference establish the principal axes, parallel and orthogonal to the high-index inclusions each one. The figure 2.1 shows an example of the cross section of a hybrid PCF, on the right, but there are many different possibilities [8].

In this project a LMA hybrid PCF with 36 μm diameter core is used as a FUT. Its inner cladding consists of an array of 1.6 μm diameter airholes with 9.3 μm distance between centers, where in the central row instead of airholes there are 6.6 μm diameter germanium-doped silica rods with numerical aperture 0.29. The airholes provide index-guiding, while bandgap guidance is given by the Ge-doped rods also. The slow axis is parallel to the row of Ge-doped silica rods and the fast axis is orthogonal. A picture of the cross-section can be seen in the figure 2.2. As it can be seen, the small black dots represent the airholes and the large black dots represent the Ge-doped rods.

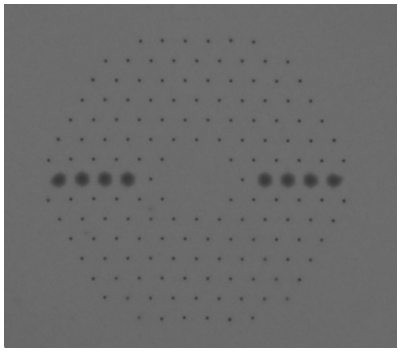

Figure 2.2: Cross-section image of the LMA hybrid PCF used in the experimental setup as a FUT. In the cladding, the small black dots are the airholes while the large ones are the Ge-doped silica rods.

In figure 2.3 an unpolarized white light transmission spectrum of a 5 m hybrid PCF piece is shown. Three transmission bands are observed at the spectral locations 680-730 nm, 810-900 nm and 980-1190 nm. Furthermore, the red edge of a transmission band is seen at 615 nm and at 1400 nm the blue edge of another transmission band. On the other hand, polarized whitelight transmission spectra are seen in figure 2.4. The transmission band for y-polarized wave is: 970 nm - 1185 nm, and for x-polarized wave is: 985 nm - 1190 nm. In this figure, "x-pol" corresponds to whitelight polarized along the slow axis and "y-pol" corresponds to whitelight polarized along the fast axis. The transmission band of y-polarization is shifted 5-10 nm to the blue edge, respect to the x-polarization, due to fiber birefringence.

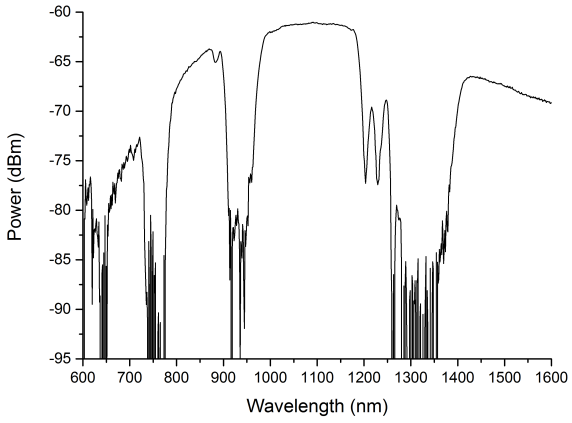

Figure 2.3: Unpolarized white light transmission spectrum of the 5 m hybrid photonic crystal fiber used in the experiments.

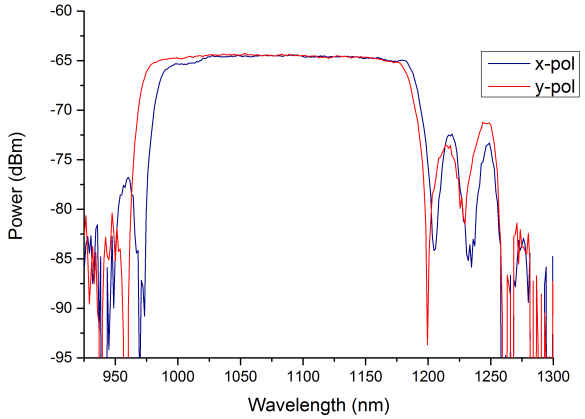

Figure 2.4: Polarized white light transmission spectra along the two principal axes of the fiber in the transmission band from 970 nm to 1190 nm.

To perform these white light measurements, white light from a Halogen-Tungsten lamp is coupled to the core of the hybrid PCF. The core light is collected with a pick-up fiber with a high numerical aperture (HNA) and a mode field diameter (MFD) of 20 μm.

Chapter 3

Four Wave Mixing

Four Wave Mixing is a third order nonlinear effect that requires a nonlinear medium (normally an optical fiber) which allows interaction between the optical waves. It is considered a parametric process because it occurs through the modulation of a medium parameter, the refractive index. Two input frequency components ω_{p1} and ω_{p2}, the pumping waves, are annihilated during the process, taking the system into a virtual state, while two new frequency components ω_s and ωi, the signal and the idler waves, relax the system when they are generated. In the case of a degenerate FWM process, the two pumping photons are at the same frequency, as the figure 3.1 shows [9].

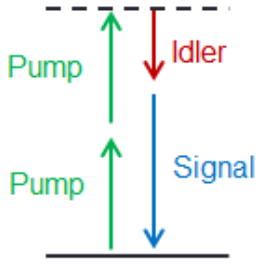

Figure 3.1: Degenerate FWM process, where two photons at the same frequency are annihilated and signal and idler waves are generated.

3.1 Main Theory

FWM must fulfill the energy conservation criterion, so the relation $\omega_{p1}+\omega_{p2} = \omega_s+\omega_i$ must be satisfied. Since degenerate FWM is considered in this project, $\omega_{p1} = \omega_{p2} = \omega_p$, what leads to the formula: $2\omega_p = \omega_s + \omega_i$. The two new photons, signal and idler, are located in a simetrical way with a frequency shift $\Omega_s = |\omega_p - \omega_s| = |\omega_p - \omega_i|$. This new components are also called Stokes

and anti-Stokes bands, being the first one the low-frequency sideband and the second one the high-frequency one [9, 10, 11].

There is a phase-matching requirement for the process to occur, which is $\Delta k = \beta_s + \beta_i - 2\beta_p = (\tilde{n}_s\omega_s + \tilde{n}_i\omega_i - 2\tilde{n}_p\omega_p)/c = 0$, where $\tilde{n}_j$ is the effective mode index at frequency ω_j. The smallest the phase mismatch the better for the process to be efficient [9, 10, 11, 3, 12].

When the pump frequency ω_p incises into the fiber, signal ω_s and idler ω_i components can be generated from noise, if the phase-matching condition is accomplished. Nevertheless, in case of a signal wave going into the fiber beside the pump wave, a new idler is created, but also the signal is amplified at the same time because of the parametric gain [9, 10].

To attain the expression of the parametric gain, the starting point are the coupled amplitude equations, considering that the pump waves are way more intense than signal and idler waves and an undepleted pump regime [9, 10, 11, 12]:

$$\frac{\delta A_p}{\delta z} = i\frac{n_2\omega_p}{c} f_{pp}|A_p|^2 A_p \tag{3.1}$$

$$\frac{\delta A_s}{\delta z} = i\frac{n_2\omega_s}{c}[2f_{sp}|A_p|^2 A_s + f_{sipp}A_p^2 A_i^* e^{-i\Delta kz}] \tag{3.2}$$

$$\frac{\delta A_i}{\delta z} = i\frac{n_2\omega_i}{c}[2f_{ip}|A_p|^2 A_i + f_{sipp}A_p^2 A_s^* e^{-i\Delta kz}] \tag{3.3}$$

where

$$f_{jk} = \frac{\langle |F_j^2||F_k^2| \rangle}{\langle |F_j^2| \rangle \langle |F_k^2| \rangle} \tag{3.4}$$

and

$$f_{sipp} = \frac{\langle F_s F_i F_p F_p \rangle}{\sqrt{\langle |F_s^2| \rangle \langle |F_i^2| \rangle \langle |F_p^2| \rangle \langle |F_p^2| \rangle}} \tag{3.5}$$

In these equations, A_p, A_s and A_i are the pump, signal and idler amplitudes, n_2 is the nonlinear index coefficient, c is the speed of light, and f_{jk}, with $jk = sp, ip, pp$, and f_{sipp} are the field overlap integrals. The angle brackets denote integration over the transverse coordinates x and y and F stands for the transverse modal distribution [9, 10, 11, 12].

Assuming $n_2\omega_s/c \approx n_2\omega_i/c \approx n_2\omega_p/c$, the expression for the parametric gain is given by the formula [9, 10, 11, 13]:

$$g = \sqrt{(\frac{n_2\omega_p}{c} P_p f_{sipp})^2 - (\frac{\kappa}{2})^2} \tag{3.6}$$

where κ is the effective phase mismatch and has the following expression:

$$\kappa = \Delta k + 2\frac{n_2\omega_p}{c} P_p(f_{sp} + f_{ip} - f_{pp}) \tag{3.7}$$

$P_p = |A_p(0)|^2$ is the pump power when $z = 0$ and κ is the effective phase mismatch which includes nonlinear contributions. Given the fact that the

sum of the field overlap integrals can be either positive or negative, κ can be negative. Hence, the phase mismatch limits for the parametric gain to be real is [13]:

$$\Delta k > -2\frac{n_2\omega_p}{c}P_p(f_{sipp} + f_{sp} + f_{ip} - f_{pp}) \tag{3.8}$$

$$\Delta k < 2\frac{n_2\omega_p}{c}P_p(f_{sipp} - f_{sp} - f_{ip} + f_{pp}) \tag{3.9}$$

In case of working with single-mode fibers, either step-index or Photonic Crystal Fiber (PCFs), the mode is well confined to the core independently of the frequency and the core area is roughly equivalent to the effective area, A_{eff}. Therefore, the field overlap integrals can be approximated as the inverse of A_{eff}. In this case, the phase mismatch range for the parametric gain to be real is [13]:

$$-4\frac{n_2\omega_p}{cA_{eff}}P_p < \Delta k < 0 \tag{3.10}$$

In this project the pump polarization is orthogonal to signal and idler polarizations, so due to polarization effects the coupled amplitude equations change as it follows [13]

$$\frac{\delta A_p}{\delta z} = i\frac{n_2\omega_p}{3c}f_{pp}|A_p|^2A_p \tag{3.11}$$

$$\frac{\delta A_s}{\delta z} = i2\frac{n_2\omega_s}{3c}[2f_{sp}|A_p|^2A_s + f_{sipp}A_p^2A_i^*e^{-i\Delta kz}] \tag{3.12}$$

$$\frac{\delta A_i}{\delta z} = i2\frac{n_2\omega_i}{3c}[2f_{ip}|A_p|^2A_i + f_{sipp}A_p^2A_s^*e^{-i\Delta kz}] \tag{3.13}$$

where the field overlap integrals remain the same. However, the gain and effective phase mismatch are also affected by the polarization [13, 14]:

$$g = \sqrt{(\frac{n_2\omega_p}{3c}P_pf_{sipp})^2 - (\frac{\kappa}{2})^2} \tag{3.14}$$

$$\kappa = \Delta k + 2\frac{n_2\omega_p}{c}P_p(\frac{1}{3}f_{sp} + \frac{1}{3}f_{ip} - f_{pp}) \tag{3.15}$$

This means that the phase mismatch limits for the parametric gain to be real, for orthogonally polarized waves, are:

$$\Delta k > -2\frac{n_2\omega_p}{c}P_p(\frac{1}{3}f_{sipp} + \frac{1}{3}f_{sp} + \frac{1}{3}f_{ip} - f_{pp}) \tag{3.16}$$

$$\Delta k < 2\frac{n_2\omega_p}{c}P_p(\frac{1}{3}f_{sipp} - \frac{1}{3}f_{sp} - \frac{1}{3}f_{ip} + f_{pp}) \tag{3.17}$$

and, finally, the range of the phase mismatch is:

$$0 < \Delta k < 4\frac{n_2\omega_p}{3cA_{eff}}P_p \tag{3.18}$$

3.2 Phase-Matching

In a FWM process, the parametric gain is maximum if the phase mismatch is null. The condition for the phase mismatch is: $\kappa = \Delta k_M + \Delta k_W + \Delta k_{NL} = 0$, where Δk_M represent the phase mismatch due to the material dispersion, Δk_W the phase mismatch due to the waveguide dispersion and Δk_{NL} the mismatch because of nonlinear effects. Splitting the effective mode index $\tilde{n}_j$ into $n_j + \Delta n_j$, the contributions to κ are:

$$\Delta k_M = (n_s\omega_s + n_i\omega_i - 2n_p\omega_p)/c \tag{3.19}$$

$$\Delta k_W = (\Delta n_s\omega_s + \Delta n_i\omega_i - (\Delta n_p + \Delta n_2)\omega_p)/c \tag{3.20}$$

$$\Delta k_{NL} = n_2\omega_p P_p/cA_{eff} \tag{3.21}$$

where one of them must be negative to fulfill the condition [9].

Using the expansion in Taylor series around the pump frequency ω_p, which is $\beta_\omega = \beta_p + (\omega - \omega_p)\beta_1 + \frac{1}{2}(\omega - \omega_p)^2\beta_2 + \frac{1}{6}(\omega - \omega_p)^3\beta_3 + ...$, another expression for the material dispersion contribution to mismatch is: $\Delta k_M \approx \beta_2\Omega_s^2 + (\beta_4/12)\Omega_s^4$, being β_2 and β_4 dispersion parameters at pump frequency, ω_p. This expression can be approximated to $\beta_2\Omega_s^2$ if the pump wavelength λ_p is not too close to the zero-dispersion wavelength (ZDW) λ_0. Thus, Δk_M is positive in the visible and the near-infrared region because, for $\lambda_p < \lambda_0$, $\beta_2 < 0$ [9].

3.2.1 Single-Mode Fibers

There are three techniques to reach the phase matching in single-mode fibers, where the waveguide dispersion contribution is small, but when working near the ZDW. One way is to use low pump powers and small frequency shifts to reduce Δk_M and Δk_{NL}. Even though κ is not exactly zero, FWM can still occur depending on the length of the fiber. The frequency shifts are related to the coherence length, which the length of the fiber should not surpass, through the formula:

$$L_{coh} = \frac{2\pi}{|\Delta k_M|} = \frac{2\pi}{|\beta_2|\Omega_s^2} \tag{3.22}$$

If the condition $L_{fib} < L_{coh}$ is satisfied, FWM can occur [9].

Another way to attain the phase matching condition is to operate in a certain range of pump wavelengths close to the ZDW. In this range, Δk_M starts to take negative values for silica around 1.28 μm and Δk_M take positive values around 1.3 μm, so the sum of the different contributions is balanced for some values of frequency shifts [9].

The last option is to work in the anomalous group velocity dispersion (GVD) regime, where the sum $\Delta k_M + \Delta k_W$ is negative because $\lambda_p \gg \lambda_0$, so

it is compensated with Δk_{NL}. In this regime, the frequency shift is related to the pump power according to the formula [9]

$$\Omega_s = \sqrt{2n_2\omega_p P_p/cA_{eff}|\beta_2|} \tag{3.23}$$

3.2.2 Birefrigent Fibers

In single mode-fibers, there is a technique to achieve phase matching exploiting modal birefringence. When different waves go through the fiber with orthogonal polarizations, the fiber suffers changes in the slow and fast axes refractive indices: $\delta n = \Delta n_x - \Delta n_y$ [9].

The phase mismatch due to the waveguide dispersion is now dominated by δn. Considering the Δk_{NL} negligible, phase matching happens when Δk_M and Δk_W are balanced. In case that the pump wavelength is in the visible region ($\lambda_p < \lambda_0$), β_2 is positive so Δk_M is also positive. To cancel Δk_M, Δk_W must be negative, what can be attained polarizing signal and idler waves along the fast axis, and the pump one along the slow axis. Thus, $\Delta n_p = \Delta n_x$ and $\Delta n_s = \Delta n_i = \Delta n_y$, which combined with $\omega_s + \omega_i = 2\omega_p$, means that the expression of Δk_W is now [9]:

$$\Delta k_W = [\Delta n_y(\omega_s + \omega_i) - 2\Delta n_x\omega_p]/c = -2\omega_p\delta n/c \tag{3.24}$$

For Δk_M and Δk_W to cancel each other, the frequency shift must be as follows [9]

$$\Omega_s = \sqrt{4\pi\delta n/(\beta_2\lambda_p)} \tag{3.25}$$

3.3 Parametric Amplification

In optical fibers, the parametric gain is used for creating fiber optical parametric amplifiers (FOPA) and fiber optical parametric oscillators, which are FOPAs with a cavity that assures continuous feedback. In an optical amplifier, the bandwith where it can supply a constant gain is a very important property [9].

Starting from boundary conditions, and assuming signal and idler launched at $z = 0$, the constants a_s and b_s fulfill:

$$a_s + b_s = B_s(0), \quad g(a_s - b_s) = (i\kappa/2)(a_s + b_s) + i\gamma P_p B_i^*(0) \tag{3.26}$$

where $\gamma \approx n_2\omega_p/cA_{eff}$. The solution to these equations gives:

$$a_s = \frac{1}{2}(1 + i\kappa/2g)B_s(0) + iC_0B_i^*(0) \tag{3.27}$$

$$b_s = \frac{1}{2}(1 - i\kappa/2g)B_s(0) - iC_0B_i^*(0) \tag{3.28}$$

where $C_0 = (\gamma P_p/2g)$. Similarly, a_i and b_i constants can be found. With them, the signal and idler fields at a certain z distance can be found and, consequently, using the relation $P_i(z) = P_s(z) - P_s(0)$, the signal and idler power versus distance expressions [9]

$$P_s(z) = P_s(0)[1 + (1 + i\kappa^2/4g^2)\sinh^2(gz)] \tag{3.29}$$

$$P_i(z) = P_s(0)(1 + i\kappa^2/4g^2)\sinh^2(gz) \tag{3.30}$$

The single pass amplification factor for the signal wave is:

$$G_s = P_s(L)/P_s(0) = 1 + (\gamma P_p/g)^2\sinh^2(gL) \tag{3.31}$$

being $P_s(L)$ the output signal power after L fiber length and $P_s(0)$ the input signal power [9, 11, 3].

The parametric gain depends on the phase mismatch, therefore, it depends on the pump frequency and the dispersive properties of the fiber, meaning that tailoring the fiber dispersion and selecting carefully the pump frequency, the FOPA bandwith can be managed [9].

The range of ω_s where G_s is above 50% of its peak value defines the amplifier bandwidth $\Delta\Omega_A$. Being $\kappa = \Delta k + 2\gamma P_p$, where $\Delta k \approx \beta_2\Omega_s^2$, with $\Omega_s = |\omega_p - \omega_s|$, the peak value is reached for $\kappa = 0$. Therefore, the peak is found for $\Omega_s = \sqrt{2\gamma P_p/|\beta_2|}$ [9].

The gain bandwidth is established by the fiber length in long fibers for a phase mismatch of $\kappa_m = 2\pi/L$. Assuming $\Delta\Omega_A \ll \Omega_s$ and using $\kappa_m = \beta_2(\Omega_s + \Delta\Omega_A)^2 + 2\gamma P_p$ the gain bandwidth results [9]

$$\Delta\Omega_A = \frac{\pi}{|\beta_2|\Omega_s L} = \frac{\pi}{L}(2\gamma P_p|\beta_2|)^{-1/2} \tag{3.32}$$

However, for short fibers, the gain bandwidth is limited by the nonlinear effects and the parametric gain disappears for $\kappa_m = 2\gamma P_p$. The FOPA bandwidth is then approximated by [9]

$$\Delta\Omega_A \approx \frac{\gamma P_p}{|\beta_2|\Omega_s} \equiv \sqrt{\frac{\gamma P_p}{2|\beta_2|}} \tag{3.33}$$

3.3.1 Parametric Oscillators

Making a laser by pumping a fiber placed inside an optical cavity with a single pump source is one application of the parametric gain. At first, the signal and idler waves are generated from noise through spontaneous FWM, given the fact that no signal beam is launched, at frequencies according to the phase-matching condition. When the recirculation is closed with the idler reentering the fiber, both signal and idler are amplified through stimulated FWM, which is the main goal in a FOPO. Finally, the signal and idler beams

are simultaneously emitted at frequencies that are symmetrically situated on opposite sides of the pump frequency. These lasers are known as parametric oscillators[9].

In the manufacturing of parametric oscillators (POs), the use of highly nonlinear fibers is common since 2001. POs can either operate endlessly with a narrow linewidth or, by pumping them with an appropriate pulsed source, they can emit a train of short pulses. In FOPOs that emit femtosecond pulses and are tunable over a wide wavelength range, it is fundamental the use of FWM [9].

3.3.2 Parametric Gain Simulations

Using the formulas for the undepleted pump regime with signal and idler orthogonal waves to pump, some calculations were run, using the Matlab files in the appendix A. These are the results:

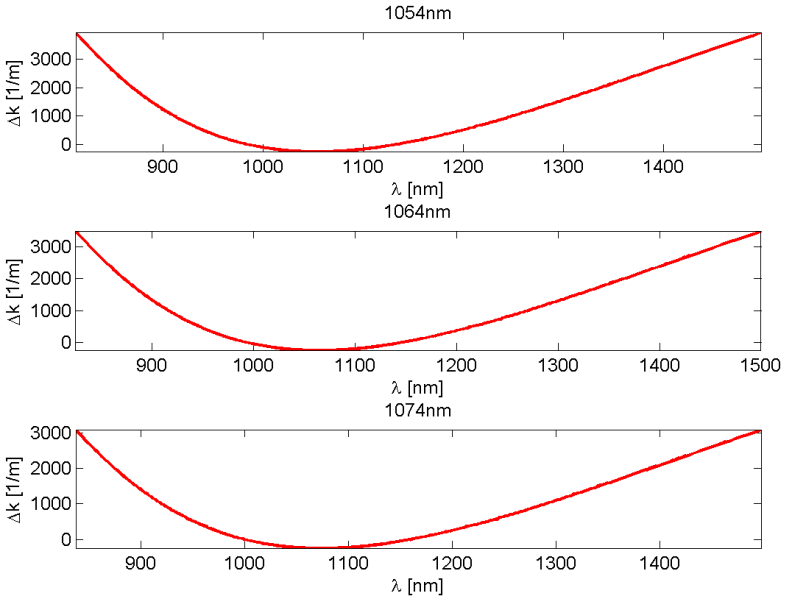

Figure 3.2: Plots for the phase mismatch considering an undepleted pump regime and signal and idler orthogonal waves to pump, for different pump wavelengths.

As expected, if we focus in the case for the pump wavelength at 1064 nm, the phase mismatch and the effective mismatch are zero for the pump wavelength, condition required for the FWM to occur, and the gain plot shows FWM components near 1000 nm and 1140 nm. Checking the other two cases, both Δk and κ are also 0 for the pump wavelengths, but the FWM components

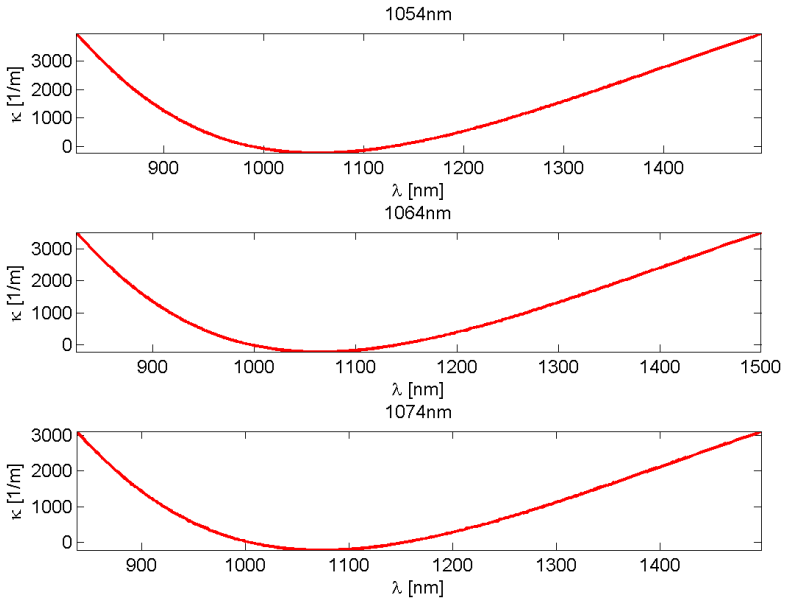

Figure 3.3: Plots for the effective phase mismatch considering an undepleted pump regime and signal and idler orthogonal waves to pump, for different pump wavelengths.

in the gain plot are red-shifted for the higher pump and blue-shifted for the lower pump as it was expected too.

The spectral position of the gain peaks for a pump wavelength of 1064 nm in figure 3.4 will be compared with the experimentally obtained gain peaks in chapter 4 section 2, where the experimental results are presented.

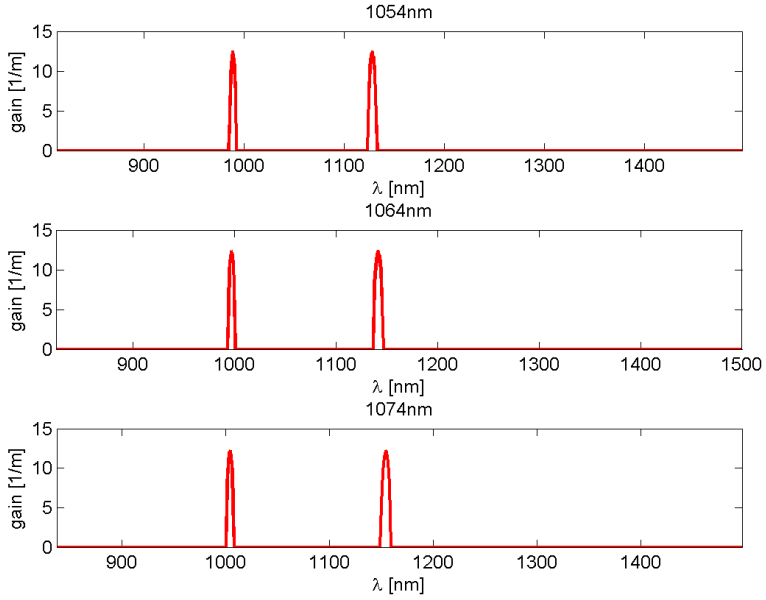

Figure 3.4: Plots for the parametric gain considering an undepleted pump regime and signal and idler orthogonal waves to pump, for different pump wavelengths.

Chapter 4

Laboratory Work

In this chapter, the most important part of the project is presented: the experimental work in the laboratory. It is divided in three sections: a first one where the two stages of the setup -the Fiber Optical Parametric Amplifier (FOPA) and the Fiber Optical Parametric Oscillator (FOPO)- are explained, another one for the laser and the FOPA characterization and the last one talking about the process to establish the recirculation.

4.1 The setup

The FOPA setup consisted of the laser, two half wave plates, a Polarizing Beamsplitter Cube (PBC) and a 1064nm filter, the fiber under test (FUT) explained at the end of chapter 3, two lenses and the characterization stage, as shown in the figure 4.1. The main goal of this part of the setup was to generate from two photons at 1064nm, two new ones at 1000nm and 1140nm.

The half wave plates, the PBC and the filter were used to make sure that there was only a well characterized 1064nm component going into the FUT, and that the polarization of this component was horizontal, in order to have a perfect coupling at the fiber input, which had the Ge-doped rods orientated in the horizontal axis.

The characterization stage consisted of a wedge reflecting 4% of the light and a device to collect the beam, which was either a camera, to check that the light was well confined in the core of the fiber, or an integrating sphere connected to an Optical Spectrum Analyzer, to help in the alignment process checking the amount of power after the FUT to see if the coupling was good enough. The point in using the wedge was to avoid that a high amount of power could burn the camera detector, which was sensitive.

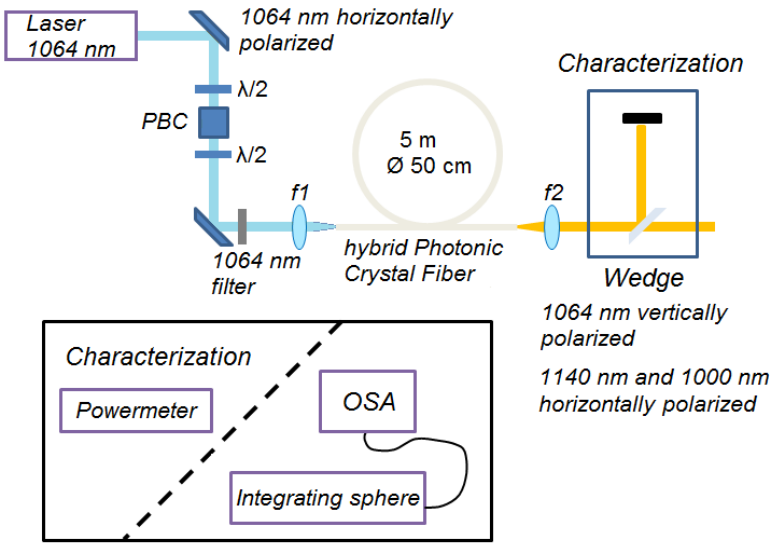

Figure 4.1: First setup, with a 5 m fiber piece as a fiber under test, consisting of the laser, the wave plates, the PBC and the filter before the FUT, and the characterization stage at the end.

4.1.1 FOPO

The final setup looked like figure 4.2. The recirculation circuit had to fulfill one condition: in order to have the FOPO working with the best conversion efficiency possible, the recirculating pulse had to spend enough time in this circuit to reach the input of the FUT at the same time that a new pumping pulse.

After the FUT, a PBC was used to separate the vertical and the horizontal polarizations because it was interesting to separate the FWM components, which were generated in the fast axis so they were horizontally polarized, from the pump and the Raman components. The components with vertical polarization were reflected in the PBC and the ones with horizontal polarization went through it, reaching a prism used to separate spatially the different components. The reason for this was to only recirculate the 1000 nm component and spatially filter out Raman scattering and light at any other wavelength than 1000 nm. In this point, the alignment for all the optical devices was focused on the 1000nm wavelength.

After the beam was divided in the different wavelengths, using two mirrors, the 1000 nm component was led into an LMA PM 15 fiber. This was a single mode, low loss, polarization maintaining fiber. It had a 15 μm core diameter and two Boron-doped silica regions to give birefringence. It was acting as a delivery fiber, its only function was to delay the pulses before

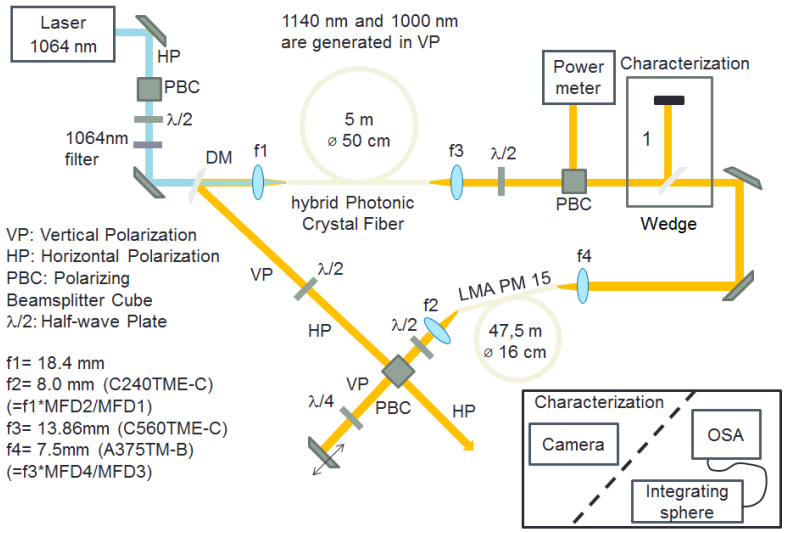

Figure 4.2: Schematic of the whole final setup

reentering the FUT. It was very important to use a PM fiber since the FWM was generated as linearly polarized light, so it was needed to keep it linearly polarized when it reentered the FUT because the FWM light that would be generated through stimulated FWM also would be linearly polarized. Without a PM LMA polarization would be lost and the recirculating component could be circularly polarized when reaching the FUT input, what means that only a fraction of the recirculating wave would still be linearly polarized for using in stimulated FWM. Hence, the fraction of backcoupled FWM, which would not be linearly polarized along the fast axis of the FUT, would not generate any stimulated FWM, so the polarization needed to be maintained to ensure the use of the whole fraction of the backcoupled FWM for stimulated FWM.

When the pulse got out of the fiber, it was directed to a rail stage. First of all, another PBC was used to separate again the polarizations, because the orientation of the dummy fiber was unknown, so even though the polarization was still linear, it was not possible to guess the orientation of the polarization of the pulse at the output. After the PBC, there was a quarter wave plate and a silver mirror. The role of the silver mirror was to tune the delay of the recirculating FWM component, since it could be moved along the rail. The point in using the quarter wave plate was to introduce a phase shift of $\lambda/4$, so after going through the plate, being reflected in the mirror and travelling across the plate again, the polarization got a π-radian phase delay, changing from horizontal to vertical polarization or vice versa. Hence, when the pulse met again the PBC, this time was not going through it but reflected 90 degrees in direction to a Dichroic Mirror, so as to get back into the main circuit and reach the input of the FUT. The dichroic mirror had particular specifications to fit the setup: it was highly transmissive for wavelengths from 1040 nm to

1130 nm and highly reflective from 900 nm to 990 nm, so it permitted the pump pulses from the laser go through it and reflected the 1000 nm FWM component. It also had an anti-reflecting coating for wavelengths from 1040 nm to 1130 nm.

At the end, the prism was removed from the setup. Also, the last stage of the recirculating circuit was turned 45 degrees. The main reason is that the DM had the optimum working point at 45 degrees between the recirculating beam and the pumping pulse, instead of 90 degrees as it was in the beginning. Moreover, a pair of half-wave plates were placed after the FUT and after the LMA in order to maximize the transmission through the PBC on the rail.

4.2 Laser and FOPA characterization

First of all, the laser was checked to be set to work with the parameters needed. The idea was to use a 1064nm, Ytterbium-doped fiber laser with a 4MHz repetition rate and a 40ps pulse width. With the help of the oscilloscope and the OSA, this parameters were tested to be correct.

It is plain to see in the figure 4.3 that the laser pumping wavelength was well set at 1064nm, but with a bit of broadening due to self-phase modulation (SPM) for high values of power. On the other hand, taking a look at the figure 4.4, it can be seen that the period was a bit less than 250ns, actually it was 242.65ns, which means that the repetition rate was 4.12MHz aprox, a bit more than expected but close enough.

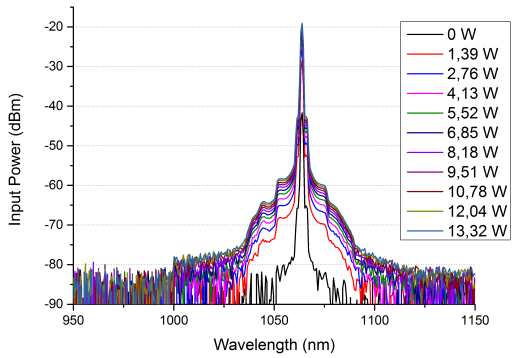

Figure 4.3: Laser spectrum. Some broadening can be appreciated due to self-phase modulation.

The first experiment that was run in the setup involved the 30 cm fiber piece as a Fiber Under Test. This fiber was a piece of a LMA hybrid PCF, which special design allowed the FWM process to occur. The fiber was not long enough to get some spontaneous FWM. Actually, there was some strange behaviour in the setup, but not the FWM components expected. The figure

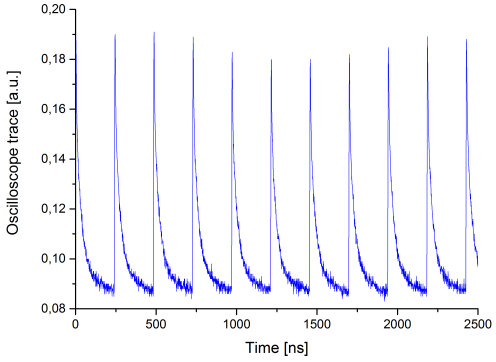

Figure 4.4: Laser oscilloscope trace

4.5 shows this behaviour around 840 nm and 1090 nm wavelengths, but mostly in the first one. It was not FWM as it can be seen in the figure, because energy conservation criterion would not be fulfilled, as there was no other components at the red edge of the spectrum. For the 840 nm component, another one around 1420 nm should arise to be sure that it was FWM. However, a solution had to be found for the setup to work as it was expected.

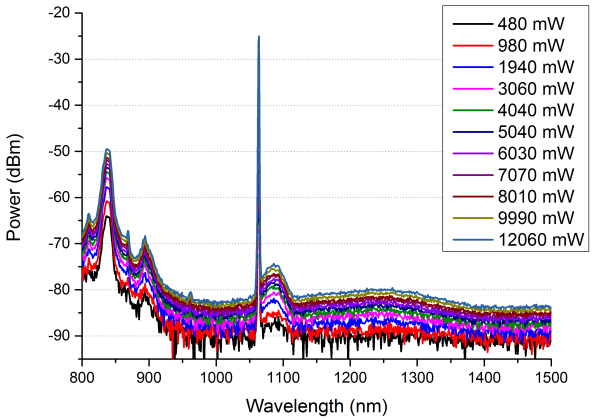

Figure 4.5: Power spectrum after the 30 cm fiber piece as FUT for different power input values. No FWM is observed, but some strange behaviour occurs around 840 nm.

Since the 30 cm fiber piece was unable to generate the desired FWM components, the decision was to use a longer one and the best option was a 5m-long one. With the new fiber in the setup, the experiments were run again. The FWM components were generated in the fast axis of the fiber, which was

the one orthogonal to the Ge-doped rods, while the pumping wavelength kept its polarization -parallel to the Ge-doped rods- and the Raman Scattering component was generated in the slow axis, so it had the same polarization as the pumping wavelength. Given the fact that the fiber output orientation was rotated 90 degrees in relation to the input orientation, the FWM components had horizontal polarization and the pump and Raman components, vertical polarization.

The output spectrum of the 5 m fiber piece is shown in figure 4.6. FWM is observed near 1000 nm and 1140 nm in good agreement with the simulations run in chapter 3 section 3, these two components were horizontally polarized, orthogonal to the pump wavelength. Also some Raman was originated near 1120 nm with vertical polarization [14].

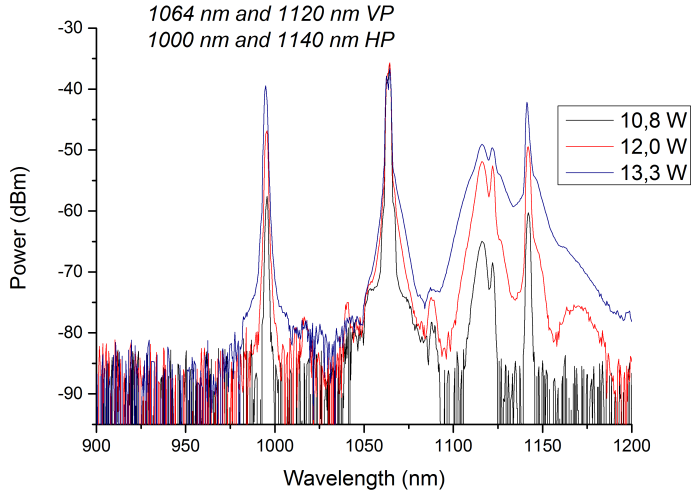

Figure 4.6: Spectrum at the output of the 5 m FUT for different input power values. There are FWM components at 1000 nm and 1140 nm with horizontal polarization. Also some Raman appears around 1120 nm with vertical polarization. The pump wavelength, 1064 nm, has also vertical polarization.

Some measurements were run to check the power and the spectrum behaviour of the FUT. On one hand, figures 4.7 and 4.8 show the power characterization of the fiber, the absolute and the relative power relations respectively between the output and the input of the fiber. Taking a look at the figure 4.8, it can be checked that the coupling was good, because it was above 70% for input power values higher than 2W. The coupling efficiency increased with pump power because the core/clad ratio of the laser improves for higher powers. This means that for higher output power from the laser there is more core light. The cladding light from the laser is not coupled to the core of the FUT, so it becomes just extra light with no use for anything. Even though for

a certain amount of power the core/clad ratio of the laser should be constant, when increasing the input power, the coupling may change due to possible heating of some optical components.

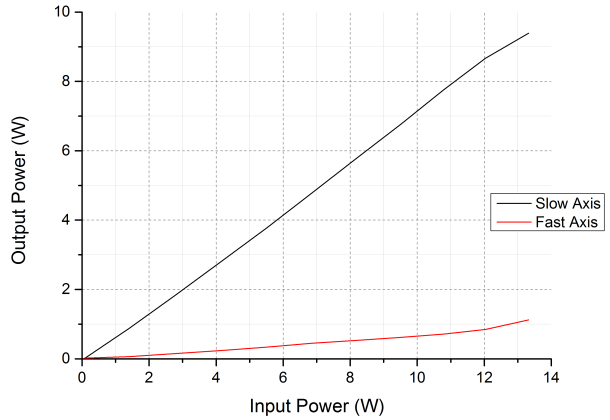

Figure 4.7: Absolute power at the output of the FUT based on the input power

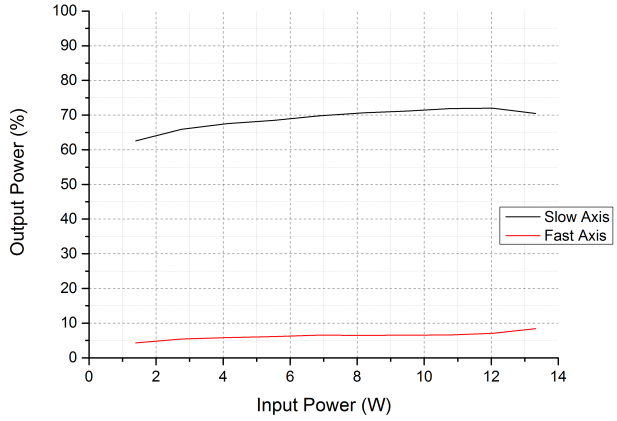

Figure 4.8: Relative power at the output of the FUT based on the input power

On the other hand, figures 4.9 and 4.10 present the fast axis and the slow axis spectra at the output of the fiber. The fast axis spectrum showed that the FWM was higher than the Raman effect, as it was expected, however it was the other way round in the slow axis. There were some other undesired, but also expected, non-linear effects also in these tests, like the weak peaks FWM components at 850nm and 1420nm, the second Raman peak at 1170nm

in the fast axis and the higher order mode (HOM) component at 1020nm in the slow axis [15].

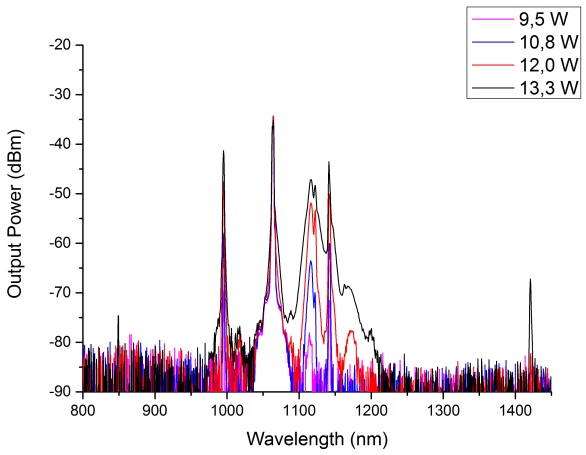

Figure 4.9: Fast axis spectrum after the FUT for different input power values. Several waves can be appreciated: pump at 1064 nm, intramodal FWM components at 1000 nm and 1140 nm, Raman at 1120 nm, intermodal FWM at 850 nm and 1420 nm and a second Raman peak at 1170 nm.

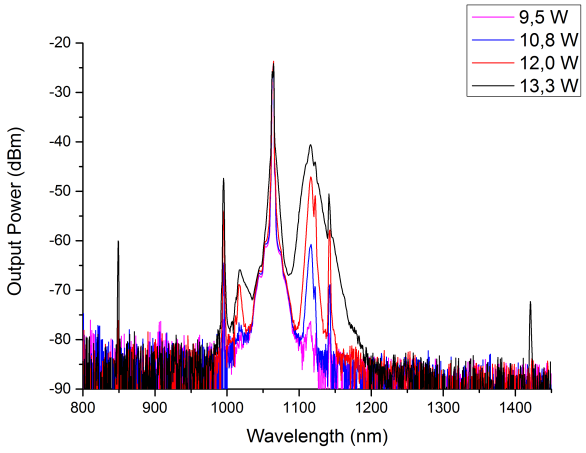

Figure 4.10: Slow axis spectrum after the FUT for different input power values. Several waves can be appreciated: pump at 1064 nm, intramodal FWM components at 1000 nm and 1140 nm, Raman at 1120 nm, intermodal FWM at 850 nm and 1420 nm and a HOM component at 1020 nm.

The 1000 nm and 1140 nm waves are birefringence assisted components, called intramodal FWM components, since they are generated in LP01 mode

or fundamental mode, same as the pump, as it can be seen in the figure 4.11. The 850 nm and 1425 nm waves are called intermodal FWM components because they are generated in a different mode (LP11), and they can also be seen in figure 4.11.

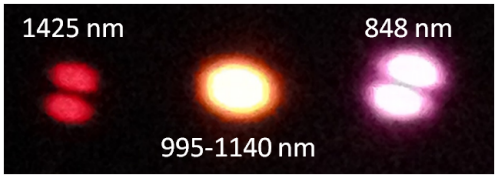

Figure 4.11: Output image of the fiber onto an IR card. Pump and intramodal FWM components are generated in LP01 mode. Intermodal FWM components are generated in LP11 mode.

4.3 Establishing the recirculation

Given the fact that FWM was plainly observed to be working in the FOPA stage, the FOPO configuration had to be established. The problem with the first trial was that the recirculating beam was not strong enough to keep its track with the IR card. Since the very beginning, the decision was to remove the prism, because with all the wavelengths travelling along the circuit it was easier to see the beam. It did not present any inconvenients, given the fact that the dichroic mirror could act as a filter, reflecting only the 1000 nm component into the FUT. The figure 4.12 shows the spectrum after the LMA. Besides the FWM, Raman and pump components, it also can be seen a second Raman peak around 1170 nm and some supercontinuum light generation close to 1200 nm, the zero dispersion wavelength of the LMA. When using maximum power, the 1000nm component was losing around 16 dB in the fiber. The amount of losses at this point of the circuit was higher than expected, so the aim was to find where to improve the setup in order to increase the available power to ease the recirculating beam alignment, because it was impossible with the OSA to visualize the FWM components.

Since the FWM components could not be seen in the OSA, it was not a viable option to help with the alignment, hence it could not be used for the timing either, so using an oscilloscope raised as a better alternative because it works in terms of time, easing to check the delay between waves. The idea was to use a photodiode to visualize the trace at the oscilloscope of the recirculating and the pumping pulses, so that the delay between them could be minimized.

Given the high losses that were ruling the setup, this option was also dismissed. The reason for this was that the two pulses would not overlap because of the difference among their voltages. In figure 4.13 the trace of the

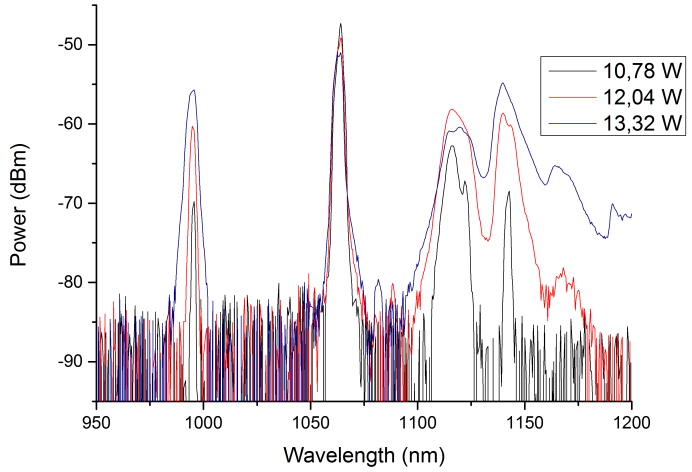

Figure 4.12: Spectrum after the LMA for different FUT input power values. Besides the FWM, Raman and pump components, it also can be seen a second Raman peak around 1170 nm and some supercontinuum light generation close to 1200 nm, the zero dispersion wavelength of the LMA.

signal after the FUT shows pulses of hundreds of mV, while the trace before the DM is lower than 10 mV. Thus, checking the figure, it is plain to see that the ground level of the signal after the FUT would mask the signal before the DM. It was time to focus on reducing the losses.

4.3.1 Losses Management

At first, the thought was that the fiber could be broken so different pieces of LMA PM fiber were used to check the values of the power before and after the LMA. Also, a High Numerical Aperture fiber was used to compare these values. The losses with the long piece of LMA PM 15 were about 16 dB, when they should be around 4 dB. The table below shows the comparison between the different fibers used to check the losses and the coupling at this point.

	LMA 47.5m	LMA 1m	LMA 0.5m	HNA 20
Losses	16.26 dB	8.98 dB	8.59 dB	1.6 dB
Coupling	2.37%	12.65dB%	13.84%	69.18%

The conclusion after these tests was that, since it was impossible to reduce enough the losses with different LMA fiber pieces but the losses were low with the HNA fiber, the problem was lying in the lenses. The lenses used at the output of the FUT and the input of the LMA were not good enough, either they were broken or the match was not the proper one for the setup to work.

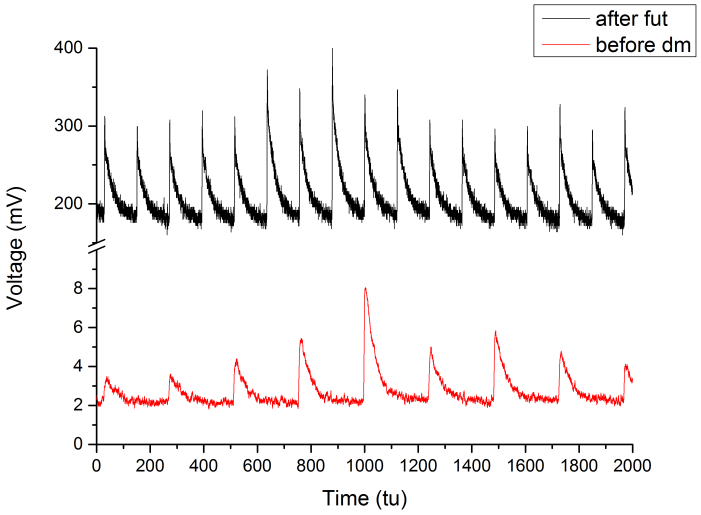

Figure 4.13: Trace comparison between the signal after the FUT and before the DM.

The lenses had to accomplish a relation between the focal length and the Mode Field Diameter (MFD), given by the formula: $f_1/f_2 = MFD_1/MFD_2$ from the equation system:
$f_1 = \pi D(MFD_1)/4\lambda \qquad f_2 = \pi D(MFD_2)/4\lambda$
where the MFD of the FUT was 25 μm and the MFD of the LMA PM fiber was 12.6 μm, what lead to the following combination of lenses:

Focal lengths (mm)				
f1	6.24	11	13.89	13.89
f2	3.1	5	6.24	7.5

After several trials, the best combination of lenses proved to be 13.89mm for the output of the FUT and 7.5mm for the input of the LMA, which proved to reduce the loss to around 4.5 dB.

4.3.2 Final Setup

Some LMA characterization was also done with the new lenses combination. The figure 4.15 shows the Polarization Extinct Ratio measurement that was done using two half wave plates, one at the input and one at the output of the LMA. The point was to maintain the beam polarization after it went through the LMA in one of the two axis, just to reduce the losses when the pulse was going through the PBC after the fiber. The chosen angle was one of the maxima of the graph in figure 4.15. The input half wave plate angle was chosen by looking on the highest power difference at the figure 4.14, so as to

have the best PER measurement. It was important that the LMA fiber had a good PER in order to be sure that the beam was the most linearly polarized possible.

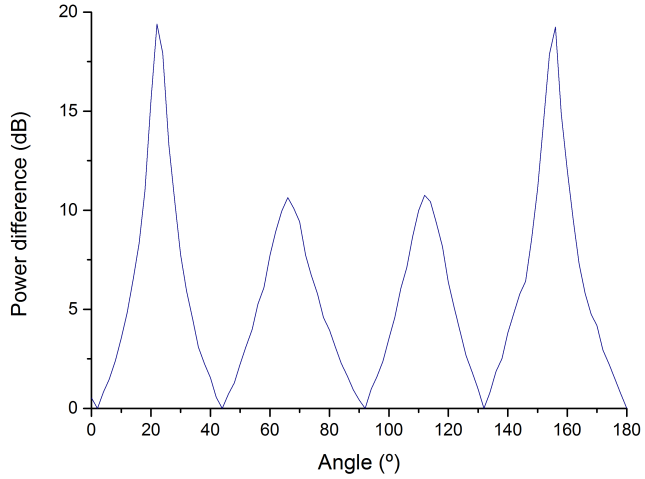

Figure 4.14: Power difference versus the input half-wave plate angle.

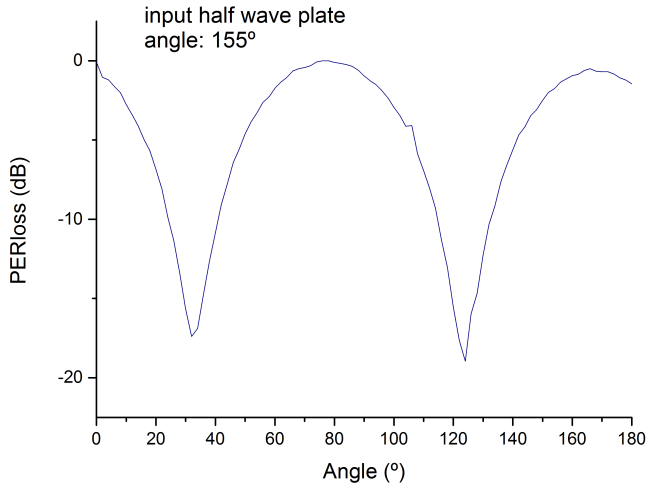

Figure 4.15: PER loss versus the output half-wave plate angle.

Furthermore, spectra measurements were also run. In the figure 4.16 a big difference between the input and the output signals are clear. Some broadening appeared at the 1000nm component, which was producing a peak power loss. Moreover, some SPM appeared at the pumping wavelength because of

the high peak power values reached at the fiber. Finally, some strange behaviour was occurring for the Raman component, the 1140nm FWM component and all the wavelengths above 1200 nm. This broad spectrum looking like supercontinuum light probably appeared since the light propagating through the LMA had high peak power components close to the zero dispersion wavelength of the LMA [16].

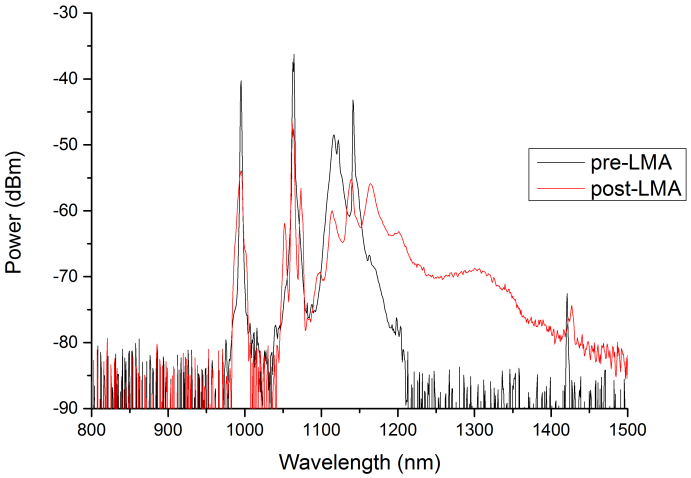

Figure 4.16: Spectra before and after the LMA.

4.3.3 External Source

After a few attempts on closing the recirculation circuit working blindly with the silver mirror at the end of the rail stage and the DM screws to try to hit the core of the FUT with the recirculating component (it was not possible to use the IR card to check the alignment for the recirculating component), the last option was to turn off the laser and use an external source after the FUT, as shown in the figure 4.17.

A tunable laser was used for this purpose. At first, some wavelengths in the visible range of the spectrum were used, but at the end the laser was tuned to wavelengths in the near-infrared, closer to the chosen FWM component for the recirculation. None of the attempts was successful, either the coupling was not good to see the beam after the LMA or the beam was not strong enough to visualize the signal in the OSA, so it was not possible to improve the alignment and the beam never reached the output of the FUT.

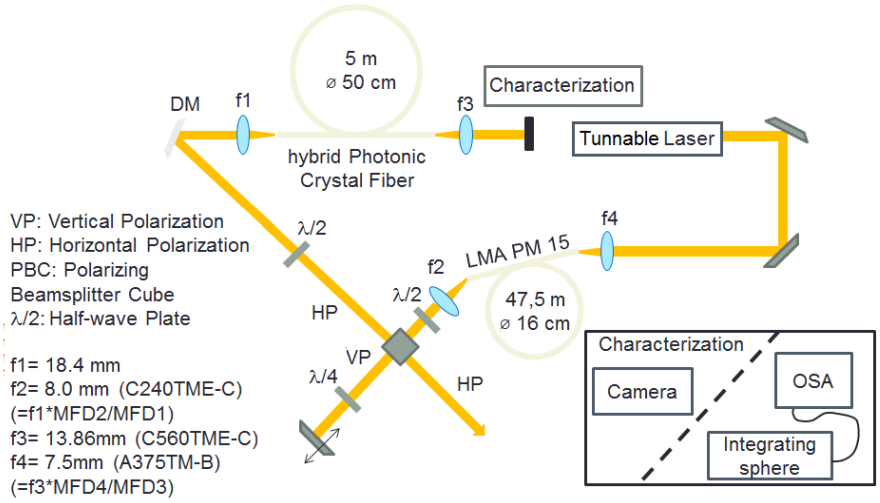

Figure 4.17: Schematic of the setup with the external source for the alignment at the last stage.

Chapter 5

Conclusion and Outlook

This project considered a FOPO configuration. There were three goals to achieve: the FOPA stage should generate the desired FWM components, the recirculation circuit should lead the FWM idler component back into the FUT and the conversion efficiency was expected to be around 40%, assuming a recirculating component going back into the fiber of 1-10 W and using the coupled differential equations governing signal, idler and pump, presented in equations (3.11)-(3.13).

As seen in chapter 5, the FOPA stage worked as expected. There was a coupling above 70% so the losses were really low, it would be difficult to improve the coupling. Some FWM was generated around 1000 nm and 1140 nm, but also Raman around 1120 nm and weak FWM components around 840 nm and 1420 nm. Raman was dominant in the slow axis, while FWM in the fast, according to what was anticipated.

However, there was not luck in the recirculation circuit. It took so long to figure out why the losses were that high after the LMA. In the end, a better combination of lenses was used, improving this issue, but still the losses could be lower. The fiber did not looked damaged, so it was not replaced. Besides, given the high peak power values going into the LMA PM, the spectrum at the output was not as good as in the input. Also, the length was not correct. The length for the LMA was calculated as follows: the period between pulses was 242.65 ns, the beam was propagating in free space along $\equiv$ 2.25 m so it spend around 7.51 ns travelling through the air (dividing distance by propagation velocity) and, with the first piece of FUT of 30 cm (the one finally used in the setup was 5-m long), being the mean refractive index around 1.46, it took 1.44 ns for the beam to cross the whole FUT. This meant that the recirculating beam should spend around 233.7 ns in the LMA fiber, what resulted in a length of 47.9 m approximately (multiplying propagation velocity by time). The biggest problem was after the LMA PM fiber. There were some unexpected losses in the PBC on the rail stage, maybe due to the output wave polarization. Also, the silver mirror was fixed in the rail, so it was easy to

lose the alignment when managing to fix the timing of the recirculating wave. Finally, when trying to reenter the recirculating component into the FUT, the pump wave was in the same path, so the IR card was not a viable option, since it could get burned. Moreover, the external source used to help in the alignment for the recirculation was not powerful enough.

5.1 Outlook

Given the possibility to continue with the project, several aspects could be improved in order to get the FOPO configuration to work, first, and to set the correct timing for the conversion efficiency reach values around 40%.

First of all, the LMA PM 15 fiber length should be recalculated using a FUT length of 5 m. Also, the prism could be reinserted in the setup, since the spectrum at the output of the fiber should be improved, a good point would be to have only the desired component into the fiber to avoid interactions that could feed unwanted nonlinear effects.

Another improvement for the setup would be the use of a stage for the silver mirror on the rail that permitted z-translation without losing the alignment while trying to fix the timing issue once the FOPO started to worked.

Finally, an external source able to work at higher power would be great to set the proper alignment for the recirculation.

Appendix A

Matlab Codes for Parametric Gain Calculations

Code for the calculations (parametric gain, phase mismatch and effective phase mismatch), where the input and output files changed for the different wavelengths used (1054 nm, 1064 nm and 1074 nm):

```
% Initiate
close all
clear all

data=load('Overlapintegral_pump_FMx_signal_idler_FMx_1.074e-06_scale.txt');
omegap=data(:,1);
omegas=data(:,2);
omegai=data(:,3);
fsipp=data(:,5);
fsp=data(:,6);
fip=data(:,7);
fpp=data(:,8);
index=size(omegap,1);

data=load('xe_ym.txt');
neffy=data(:,2);

data=load('xm_ye.txt');
neffx=data(:,2);

powp=10e3;
c=299792458;
n2=2.7*1e-16;
n2=n2/(1e2^2); %[cm^2/W] to [m^2/W]

file=fopen('gain_1.074_scaled.txt','a');

for k=1:index
    indexp=find(omegas==omegap(k));
```

```
    indexi=find(omegas==omegai(k));
    neffp=neffx(indexp);
    neffs=neffy(k);
    neffi=neffy(indexi);
    deltabeta=1./c.*(neffs.*omegas(k)+neffi.*omegai(k)-2.*neffp.*omegap(k));
    kappa=deltabeta+2.*n2.*omegap(k)./c.*powp.*(fsp(k)+fip(k)-fpp(k));
    test=((n2.*omegap(k)./c.*powp.*fsipp(k)).^2)-((kappa./2).^2);
    if test>0
        gain=abs(sqrt(test));
    else
        gain=0;
    end

    fprintf(file,'%d\t%d\t%d\t%d\t%d\n',omegas(k),neffy(k),gain,kappa,deltabeta);

end

fclose all;
```

Code for the parametric gain plots:

```
%Initiate
clear all
close all

data1=load('gain_1.054_scaled.txt');
X1=data1(:,1);
X1=1./((X1./(2.*pi))./299792458).*1e9;
Y1=data1(:,3);
data2=load('gain_1.064_scaled.txt');
X2=data2(:,1);
X2=1./((X2./(2.*pi))./299792458).*1e9;
Y2=data2(:,3);
data3=load('gain_1.074_scaled.txt');
X3=data3(:,1);
X3=1./((X3./(2.*pi))./299792458).*1e9;
Y3=data3(:,3);
subplot(3,1,1)
plot(X1,Y1,'r','Linewidth',2)
xlabel('\lambda [nm]','Fontsize',12)
ylabel('gain [1/m]','Fontsize',12)
axis([-inf inf 0 15])
set(gca,'Fontsize',12)
title('1054nm','Fontsize',12)
subplot(3,1,2)
plot(X2,Y2,'r','Linewidth',2)
xlabel('\lambda [nm]','Fontsize',12)
ylabel('gain [1/m]','Fontsize',12)
axis([-inf inf 0 15])
set(gca,'Fontsize',12)
title('1064nm','Fontsize',12)
subplot(3,1,3)
plot(X3,Y3,'r','Linewidth',2)
xlabel('\lambda [nm]','Fontsize',12)
ylabel('gain [1/m]','Fontsize',12)
axis([-inf inf 0 15])
set(gca,'Fontsize',12)
title('1074nm','Fontsize',12)
saveas(gca,'gain_simulation_v2.png')
```

Code for the phase mismatch calculation:

```
%Initiate
clear all
close all

data1=load('gain_1.054_scaled.txt');
X1=data1(:,1);
X1=1./((X1./(2.*pi))./299792458).*1e9;
Y1=data1(:,5);
data2=load('gain_1.064_scaled.txt');
X2=data2(:,1);
X2=1./((X2./(2.*pi))./299792458).*1e9;
Y2=data2(:,5);
data3=load('gain_1.074_scaled.txt');
X3=data3(:,1);
X3=1./((X3./(2.*pi))./299792458).*1e9;
Y3=data3(:,5);
subplot(3,1,1)
plot(X1,Y1,'r','Linewidth',2)
xlabel('\lambda [nm]','Fontsize',12)
ylabel('\Deltak [1/m]','Fontsize',12)
axis([-inf inf -inf inf])
set(gca,'Fontsize',12)
title('1054nm','Fontsize',12)
subplot(3,1,2)
plot(X2,Y2,'r','Linewidth',2)
xlabel('\lambda [nm]','Fontsize',12)
ylabel('\Deltak [1/m]','Fontsize',12)
axis([-inf inf -inf inf])
set(gca,'Fontsize',12)
title('1064nm','Fontsize',12)
subplot(3,1,3)
plot(X3,Y3,'r','Linewidth',2)
xlabel('\lambda [nm]','Fontsize',12)
ylabel('\Deltak [1/m]','Fontsize',12)
axis([-inf inf -inf inf])
set(gca,'Fontsize',12)
title('1074nm','Fontsize',12)
saveas(gca,'deltabeta_v2.png')
```

Code for the effective phase mismatch calculation:

```
%Initiate
clear all
close all

data1=load('gain_1.054_scaled.txt');
X1=data1(:,1);
X1=1./((X1./(2.*pi))./299792458).*1e9;
Y1=data1(:,4);
data2=load('gain_1.064_scaled.txt');
X2=data2(:,1);
X2=1./((X2./(2.*pi))./299792458).*1e9;
Y2=data2(:,4);
data3=load('gain_1.074_scaled.txt');
X3=data3(:,1);
X3=1./((X3./(2.*pi))./299792458).*1e9;
Y3=data3(:,4);
subplot(3,1,1)
plot(X1,Y1,'r','Linewidth',2)
xlabel('\lambda [nm]','Fontsize',12)
ylabel('\kappa [1/m]','Fontsize',12)
axis([-inf inf -inf inf])
set(gca,'Fontsize',12)
title('1054nm','Fontsize',12)
subplot(3,1,2)
plot(X2,Y2,'r','Linewidth',2)
xlabel('\lambda [nm]','Fontsize',12)
ylabel('\kappa [1/m]','Fontsize',12)
axis([-inf inf -inf inf])
set(gca,'Fontsize',12)
title('1064nm','Fontsize',12)
subplot(3,1,3)
plot(X3,Y3,'r','Linewidth',2)
xlabel('\lambda [nm]','Fontsize',12)
ylabel('\kappa [1/m]','Fontsize',12)
axis([-inf inf -inf inf])
set(gca,'Fontsize',12)
title('1074nm','Fontsize',12)
saveas(gca,'kappa_v2.png')
```

Bibliography

[1] Thomas Tanggaard Alkeskjold. Large-mode-area ytterbium-doped fiber amplifier with distributed narrow spectral filtering and reduced bend sensitivity. *Optics express*, 17:16394–16405, 2009.

[2] Sidsel R. Petersen, Thomas T. Alkeskjold, Federica Poli, Enrico Coscelli, Mette M. Jø rgensen, Marko Laurila, Jesper Læ gsgaard, and Jes Broeng. Hybrid Ytterbium-doped large-mode-area photonic crystal fiber amplifier for long wavelengths. *Optics Express*, 20(6):6010, 2012.

[3] Sidsel R. Petersen, Thomas T. Alkeskjold, and Jesper Læ gsgaard. Degenerate four wave mixing in large mode area hybrid photonic crystal fibers. *Optics Express*, 21(15):18111, 2013.

[4] J H Yuan, G Y Zhou, H Z Liu, C M Xia, X Z Sang, Q Wu, C X Yu, K R Wang, B B Yan, Y Han, G Farrell, and L T Hou. Coherent Anti-Stokes Raman Scattering Microscopy by Dispersive Wave Generations in a Polarization Maintaining Photonic Crystal Fiber. *Progress in Electromagnetics Research-Pier*, 2013.

[5] Robert T Murray, Edmund J. R. Kelleher, Sergei V Popov, Arnaud Mussot, Alexandre Kudlinski, and James R Taylor. Widely tunable polarization maintaining photonic crystal fiber based parametric wavelength conversion. *Optics Express*, 21(1310):15826, 2013.

[6] Ekaterina A. Zlobina, Sergey I. Kablukov, and Sergey A. Babin. Phase matching for parametric generation in polarization maintaining photonic crystal fiber pumped by tunable Yb-doped fiber laser, 2012.

[7] Jesper Lægsgaard. Introduction to dielectric waveguides. *lecture notes for course 34041, Department of Photonics Engineering, DTU*, 2012.

[8] Sidsel R. Petersen. Ytterbium-doped large-mode-area photonic crystal fiber amplifier with distributed spectral filtering for use at 1178 nm Master Project, 2011.

[9] Govind P. Agrawal. *Nonlinear fiber optics*. 2006.

[10] Jonas Hansryd, Peter a. Andrekson, Mathias Westlund, Jie Li, and Per Olof Hedekvist. Fiber-based optical parametric amplifiers and their applications. 2002.

[11] Sidsel R. Petersen, Jesper Lægsgaard, and Thomas Alkeskjold. Intermodal parametric gain of degenerate four wave mixing in large mode area hybrid photonic crystal fibers. In *Nonlinear Optics*, page NW4A.08. Optical Society of America, 2013.

[12] Sidsel R Petersen, Thomas T Alkeskjold, Christina B Olausson, and Jesper Læ gsgaard. Extended parametric gain range in photonic crystal fibers with strongly frequency-dependent field distributions. 39(16):4891–4894, 2014.

[13] Sidsel R. Petersen, Thomas T. Alkeskjold, Christina B. Olausson, and Jesper Læ gsgaard. Four-wave mixing in large mode area photonic crystal fibers. *Optics Express*, 2014.

[14] Sidsel R. Petersen, Thomas T. Alkeskjold, Christina B. Olausson, and Jesper Lægsgaard. Polarization switch of four-wave mixing in large mode area hybrid photonic crystal fibers. *Opt. Lett.*, 40(4):487–490, Feb 2015.

[15] S R Petersen, T T Alkeskjold, C B Olausson, and J Lægsgaard. Frequency conversion through spontaneous degenerate four wave mixing in large mode area hybrid photonic crystal fibers. *SPIE Photonics West 2014-LASE: Lasers and Sources*, 8961:1–7, 2014.

[16] *http://www.nktphotonics.com/files/files/LMA-PM-15.pdf*.